Metallization of magnesium polyhydrides under pressure

David C. Lonie,[1] James Hooper,[1] Bahadir Altintas,[1,2] and Eva Zurek[1,*]

[1]*Department of Chemistry, State University of New York at Buffalo, Buffalo, New York 14260-3000, USA*
[2]*Department of Computer Education and Instructional Technologies, Abant Izzet Baysal University, 14280, Golkoy, Bolu, Turkey*

Evolutionary structure searches are used to predict stable phases with unique stoichiometries in the hydrogen-rich region of the magnesium/hydrogen phase diagram under pressure. MgH_4, MgH_{12}, and MgH_{16} are found to be thermodynamically stable with respect to decomposition into MgH_2 and H_2 near 100 GPa, and all lie on the convex hull by 200 GPa. MgH_4 contains two H^- anions and one H_2 molecule per Mg^{2+} cation, whereas the hydrogenic sublattices of MgH_{12} and MgH_{16} are composed solely of $H_2^{\delta-}$ molecules. The high-hydrogen content stoichiometries have a large density of states at the Fermi level, and the T_c of MgH_{12} at 140 GPa is calculated to be nearly three times greater than that of the classic hydride, MgH_2, at 180 GPa.

I. INTRODUCTION

In 1935, Wigner and Huntington predicted that hydrogen, which exists in the paired molecular state at ambient pressures and temperatures, would become an alkali-metal-like monoatomic solid when compressed to pressures exceeding 25 GPa.[1] This turned out to be a bit of an underestimate. Structure searches based upon density functional theory calculations have identified a number of molecular ($P \leqslant 400$ GPa)[2] and quasimolecular or atomic ($P = 0.5$–5 TPa)[3,4] structures in the cold phase diagram, and experiments in diamond anvil cells show that the insulating phase III with paired hydrogens is stable over a broad temperature range and up to at least 360 GPa.[5] Recent experimental work at room temperature above 220 GPa, which showed a pronounced softening of one of the Raman active molecular vibrons upon compression,[6] and potential conductivity[7] has generated much excitement.[8] The newly discovered phase IV of hydrogen is thought to be a mixed structure composed of layers of molecular units as well as weakly bonded graphene-like sheets.[9,10] Superconductivity at pressures of 450 GPa and temperatures up to 242 K has been predicted in the molecular phase,[11] whereas the superconducting transition temperature, T_c, may approach 764 K for monoatomic hydrogen near 2 TPa.[12]

What are the structural motifs that compressed hydrogen adopts when doped with an electropositive element? Theoretical work has predicted the presence of hydridic H^- atoms, $H_2^{\delta-}$ molecules, $H^- \cdots H_2$ motifs, symmetric H_3^- molecules, polymeric $(H_3^-)_\infty$ chains, and sodalite cage structures, with the nature of the hydrogenic sublattice depending upon the identity of the alkali or alkaline earth metal, and the pressure.[13–20] The latter clathrate-like cage, which encapsulated the calcium cation in CaH_6, was shown to be susceptible to a Jahn-Teller distortion, giving rise to a remarkable electron-phonon coupling parameter of 2.69 at 150 GPa with a concomitant T_c of ∼225 K.[20]

Herein, evolutionary structure searches are used to seek out the stoichiometries and structures of magnesium polyhydrides, MgH_n with $n > 2$, under pressure. MgH_4 is predicted to become stable with respect to decomposition into MgH_2 and H_2 near 100 GPa, and it remains the most stable stoichiometry until at least 200 GPa. $Cmcm$-MgH_4 contains two hydridic hydrogens and one hydrogen molecule per Mg^{2+} cation, and it

becomes metallic as a result of pressure-induced band overlap. However, due to the low density of states at the Fermi level, the estimated T_c at 100 GPa is only ∼10 K higher than that of $P6_3/mmc$-MgH_2 at 180 GPa. Two other stoichiometries, MgH_{12} and MgH_{16}, are calculated as being thermodynamically stable at higher pressures. Because these hydrogen rich phases exhibit an "$H_2^{\delta-}$ belt" surrounding the Mg^{2+} cations, and do not contain any hydridic hydrogens, they have a high density of states at the Fermi level. Assuming typical values of the Coulomb pseudopotential, the T_c of MgH_{12} is calculated as being between 47–60 K at 140 GPa. Phases with a greater ratio of $H_2^{\delta-}$:H^- tend to have a larger density of states at the Fermi level and a higher T_c.

II. COMPUTATIONAL METHODS

The structural searches were performed using the open-source evolutionary algorithm (EA) XTALOPT release 8 along with the default parameter set.[21] Evolutionary runs were carried out on the MgH_2 stoichiometry at 0, 25, 50, 100, 150, 200, and 250 GPa with cells containing 2, 3, 4, and 8 formula units (FU). At 200 GPa, additional searches on cells with 5 and 6 FU were performed. Only the known α, ϵ, and ζ phases were recovered, with the $P6_3/mmc$ structure remaining the most stable up to the highest pressures considered. Exploratory searches at 200 GPa revealed that MgH_n with $n = 2.5, 3, 3.5, 4.5, 5, \ldots$ were noticeably less stable than those with even n. Thus a more refined search was carried out at 100 and 200 GPa, which was restricted to even n ranging from 4–16 with 2–4 FU for MgH_4 and MgH_6, 2–3 FU for MgH_8, and 2 FU otherwise. Additional searches for $n = 4$ and 6 were carried out with 8 and 5 FU at 100 and 200 GPa, respectively. Duplicate structures were detected using the XTALCOMP[22] algorithm. The SPGLIB package[23] was used to determine space-group symmetries.

Geometry optimizations and electronic structure calculations were performed using using density functional theory (DFT) as implemented in the Vienna *ab initio* simulation package (VASP).[24] The exchange and correlation effects were treated using the Perdew-Burke-Ernzerhof (PBE) functional[25] with plane-wave basis sets and a kinetic energy cutoff of 600 eV. The hydrogen $1s^1$ and magnesium $2p^63s^2$ electrons were treated explicitly and the projector-augmented wave

(PAW) method[26] was used to treat the core states. The k-point grids were chosen using the Γ-centered Monkhorst-Pack scheme. The number of divisions along each reciprocal lattice vector was chosen such that the product of this number with the real lattice constant was 40 Å for the final geometry optimizations as well as at least 50 Å for the electronic densities of states (DOS) and band structures.

In situations where band gap closure occurs as a result of pressure-induced broadening, and eventual overlap of the valence and conduction bands, standard density functionals predict too low metallization pressures. For this reason, we have calculated the DOS of select structures using the HSE06 screened hybrid functional, which has been shown to give good accuracy for band gaps.[27] Due to the immense computational expense involved in hybrid calculations, the geometries employed have been optimized with PBE. Recently, it has been shown that inclusion of Hartree–Fock exchange in functionals such as HSE06 or PBE0 can have a significant impact upon the calculated transition pressures between different phases.[28,29] Moreover, a study considering liquid nitrogen at pressures up to 200 GPa (and finite temperatures) has shown that the structural relaxations with a hybrid functional can lead to large Peierls distortions (which inevitably have an impact on the band gap).[30] It has been proposed that nontrivial exchange correlation effects can become quite important at extreme pressures, in particular when electron localization occurs ("electride" behavior),[31] and/or when the semicore electrons interact.[29] Since we do not observe significant broadening of the Mg $2p$ bands at the pressures considered here, it may be that structural relaxation with a hybrid functional will yield similar results as PBE. This will be considered in future studies. However, as expected, our calculations show that hybrid functionals increase the pressures at which band gap closure is predicted to occur.

Phonon calculations were performed using VASP combined with the phonopy package[32] on supercells of 288 (MgH_2), 160 (MgH_4), 351 (MgH_{12}), and 272 (MgH_{16}) atoms. The electronic densities of states and phonon band structures obtained with VASP for MgH_2, MgH_4, and MgH_{12} at 180, 100, and 140 GPa showed good agreement to those computed using the Quantum espresso (QE) program[33] and the computational settings described below.

In the QE calculations, the H and Mg pseudopotentials, obtained from the QE pseudopotential library, were generated by the method of von Barth and Car with $1s^1$ and $3s^2 3p^0$ valence configurations, along with the Perdew-Zunger local density approximation.[34] We choose this particular Mg pseudopotential as it has been employed in numerous lattice dynamical studies of materials under pressure, see, for example, Ref. 35. Plane-wave-basis set cutoff energies, which gave an energy convergence to better than 0.3 mRy/atom were 55, 75, and 90 Ry for MgH_2, MgH_4, and MgH_{12}, respectively, and a $16 \times 16 \times 16$ Brillouin-zone sampling scheme of Methfessel-Paxton[36] with a smearing factor of 0.02 Ry was employed. Density functional perturbation theory, which is implemented in QE, was used for the phonon calculations. The electron-phonon coupling matrix elements were calculated using a $16 \times 16 \times 16$ k mesh and $4 \times 4 \times 4$ q mesh for MgH_2 and MgH_4, along with a $12 \times 12 \times 12$ k mesh and $3 \times 3 \times 3$ q mesh for MgH_{12}. The electron-phonon

coupling (EPC) parameter λ was calculated using a set of Gaussian broadenings in steps of 0.005 Ry. The broadening for which λ was converged to within 0.005 was 0.035, 0.025, and 0.040 Ry for MgH_2, MgH_4, and MgH_{12}, respectively. The superconducting transition temperature T_c has been estimated using the Allen-Dynes modified McMillan equation[37] as

$$T_c = \frac{\omega_{\ln}}{1.2} \exp\left[-\frac{1.04(1+\lambda)}{\lambda - \mu^*(1 + 0.62\lambda)} \right], \quad (1)$$

where $\omega_{\ln}$ is the logarithmic average frequency and μ^* is the Coulomb pseudopotential, often assumed to be between $\sim$0.1–0.13.

The molecular calculations on $H_2^{\delta-}$ and MgH_{12} were performed using the ADF software package[38] and the revPBE gradient density functional. The band structures of select phases (see the Supplemental Material[39]) were calculated using the tight-binding linear muffin-tin orbital (TB-LMTO) method,[40] the VWN local exchange correlation potential along with the Perdew-Wang GGA.

III. RESULTS AND DISCUSSION

A. Squeezing MgH_2

The potential for reversible hydrogen storage has resulted in much interest not only in crystalline MgH_2, but also in nanoparticles based on the structure of the various phases of this solid.[41–45] At 1 atm, α-MgH_2 assumes a TiO_2-rutile-type geometry and it undergoes a series of structural transitions, $\alpha(P4_2/mnm) \rightarrow \gamma(Pbcn) \rightarrow \beta(Pa\bar{3}) \rightarrow \delta(Pbc2_1) \rightarrow \epsilon(Pnma)$, at 0.39, 3.84, 6.73, and 10.26 GPa.[46,47] At around 165 GPa, the $Pnma$ phase slightly distorts to a higher symmetry $P6_3/mmc$ Ni_2In-type configuration, ζ-MgH_2, see Fig. 1, which was shown to be dynamically stable at 180 GPa. At lower pressures BaH_2[48,49] CaH_2,[50] and SrH_2[51] also adopt this structure. However, whereas the heavier alkaline earth dihydrides with $P6_3/mmc$ symmetry are insulating, in MgH_2, metallization is predicted to occur by 170 GPa at the PBE-level of theory.[52] Our evolutionary runs
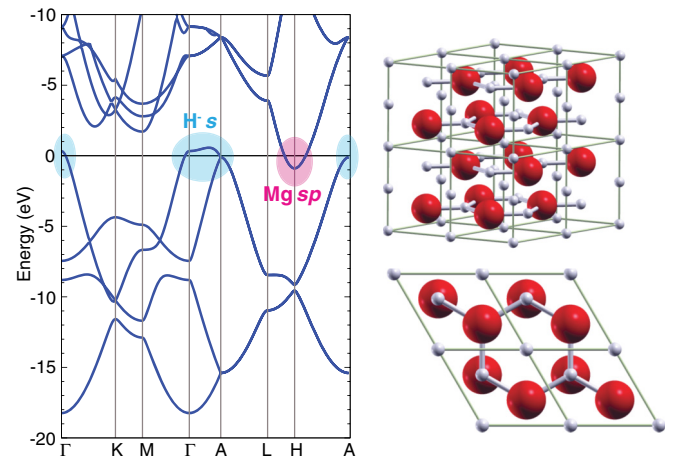

FIG. 1. (Color online) The electronic band structure of ζ-MgH_2 at 180 GPa. The character of the bands which cross the Fermi level is highlighted. The Fermi energy is set to zero in all of the plots. A side and top view of ζ-MgH_2 is shown on the right, with the Mg/H atoms colored in red/white.

did not reveal any other phases of MgH_2 up to 300 GPa, a pressure at which the metallicity in ζ-MgH_2 persists. Calculations using the HSE06 screened hybrid functional[27] confirm the metallicity at $\sim$180 GPa.

ζ-MgH_2 is metallic as a result of the closure of an indirect band gap. A flat band displaying H^- s character rises above the Fermi level E_F around Γ-A, and a steep band that boasts primarily Mg s and a little bit of Mg p character falls below E_F around the H point, as illustrated in Fig. 1. ζ-MgH_2 contains half the number of valence electrons per formula unit as does MgB_2, which becomes superconducting at 39 K.[53] The B σ and H s bands are comparable, in particular, the "holes" at the top of the band spanning from Γ to A. However, whereas MgB_2 consists of hexagonal boron sheets with Mg^{2+} intercalated in the hexagonal holes, the hexagonal network in ζ-MgH_2 is made up of alternating Mg^{2+} and H^- ions, with the second set of hydrides located in the hexagonal holes. So the Fermi surfaces arising from the B σ[54] and the H s bands[52] are not identical. We also noticed some similarities between ζ-MgH_2 and the most stable CsH phase above 160 GPa.[55] Whereas the former can be thought of as layers of graphitic sheets of alternating Mg^{2+} and H^- ions arranged in an $ABABA...$ stacking with H^- sandwiched in between the two layers, in CsH half of the H^- have been removed so that only layers of Cs^+ and H^- are found.

The density of states at the Fermi level, $g(E_F)$, of ζ-MgH_2 is 0.01 eV^{-1} per electron at 170 GPa and by 300 GPa it decreases only slightly. Despite the relatively low $g(E_F)$, we were intrigued in the possibility of superconductivity in this system. Figure 2 plots the phonon band structure and densities of states, phonon linewidths [$\gamma(\omega)$], Eliashberg spectral function [$\alpha^2F(\omega)$], and $\lambda(\omega)$ of ζ-MgH_2 at 180 GPa. 38% of the total EPC parameter, λ, is a result of the low-frequency modes below $\sim$700 cm^{-1}, which are associated primarily with the motions of the heavier Mg ions, whereas the region between 750–2400 cm^{-1}, which is mostly due to motions of the H^- anions, contributes 62% towards the total λ with the modes along Γ-K-M and H-L-A playing a dominant role. The modes above 2100 cm^{-1} are primarily caused by the set of

H^- anions, which are closer to the Mg^{2+} cations (the Mg-H distances at 180 GPa measure 1.58 and 1.81 Å). Despite the modest $g(E_F)$ the total EPC parameter is calculated as being 0.58, and along with an ω_{ln} of 1111 K gives rise to a T_c of 16–23 K for μ^* ranging from 0.13–0.1, respectively, via the Allen-Dynes modified McMillan equation. For comparison, the EPC parameter and ω_{ln} for BaH_2 in the simple hexagonal structure at 60 GPa have been calculated as being 0.22 and 780 K, respectively, giving rise to T_c on the order of only a few millidegrees Kelvin.[48]

Given the recent interest in compressed hydrogen-rich solids as potential superconductors, we began to wonder if H_2 may mix with MgH_2 under pressure and what other metallic systems may be found. As will be shown in a moment, while the ζ phase is preferred for MgH_2 above 165 GPa, it is not the most stable point on the hydrogen-rich Mg/H phase diagram at these pressures.

B. Stabilization of the polyhydrides

The first ionization potential of magnesium is $\sim$2 eV larger than that of lithium, suggesting that stabilization of the magnesium polyhydrides will occur at a somewhat higher pressure than the lithium polyhydrides (that is, above 100 GPa).[13] The ionic radius of Mg^{2+} is about 30% smaller than that of Ca^{2+}, and since CaH_4 was found to be the most stable stoichiometry at $P = 50$–150 GPa and CaH_6 at 200 GPa,[20] we may expect that the most favorable MgH_n combination has $2 < n < 6$. How do these predictions—based upon chemical intuition that was developed by analyzing computational studies of compressed polyhydrides[13–20]—compare with the results from our evolutionary structure searches?

The calculated enthalpies of formation, ΔH_F, of the important MgH_n structures found in our searches are provided in Fig. 3. At 100 GPa, only MgH_4 is predicted to resist decomposition into MgH_2 and H_2. In fact, MgH_4 persists as
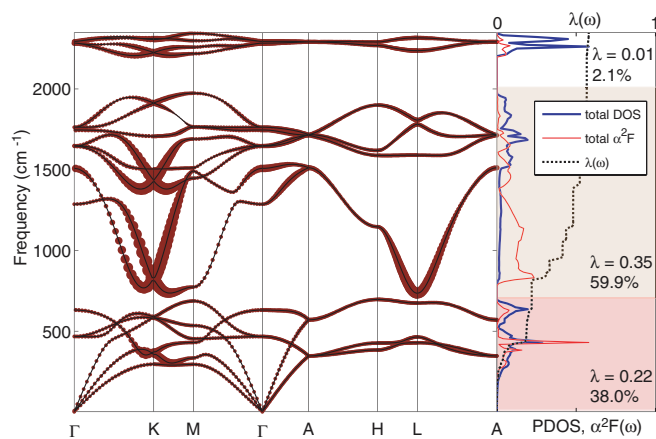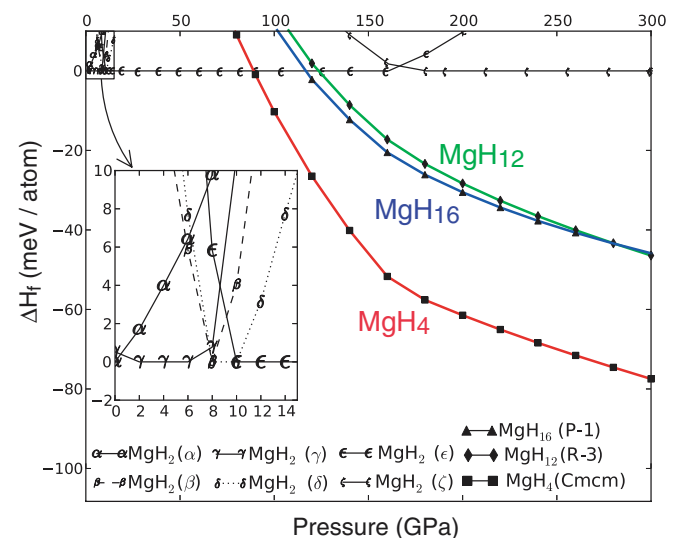

FIG. 2. (Color online) Phonon band structure, phonon density of states, and the Eliashberg spectral function, $\alpha^2F(\omega)$, of ζ-MgH_2 at 180 GPa. Circles indicate the phonon linewidth with a radius proportional to the strength. At this pressure, $\lambda = 0.58$, $\omega_{ln} = 1111$ K, and $T_c = 16$–23 K assuming $\mu^* = 0.13$–0.1.

FIG. 3. (Color online) ΔH_F of the MgH_4, MgH_{12}, and MgH_{16} phases as a function of pressure. The plot also illustrates the enthalpy of the various MgH_2 phases with respect to the most stable structure at a given pressure, with the region below 15 GPa magnified in the inset.

having the most negative ΔH_F as the pressure is increased. By 200 GPa all stoichiometries except for $MgH_{2.5}$, MgH_3, and $MgH_{3.5}$ have a negative ΔH_F. Because MgH_4, MgH_{12}, and MgH_{16} lie on the convex hull at 200 GPa, they are thermodynamically stable with respect to decomposition into other phases and MgH_2/H_2. Figure 3 illustrates that whereas the ΔH_F of MgH_4 starts to become negative near 92 GPa, for MgH_{12} and MgH_{16}, this occurs at 122 and 117 GPa, respectively. Comparison of these findings with the predictions based upon our newly developed chemical intuition under pressure illustrates that we did reasonably well in predicting the stabilization pressures and most stable stoichiometry without performing any computations. Now, let us begin our exploration of the structural peculiarities and electronic structures of the magnesium polyhydrides falling on the convex hull.

C. MgH_4: H_2 molecules and hydridic atoms

The phase with the most negative enthalpy of formation throughout the pressure range studied, $Cmcm$-MgH_4, forms a distorted CsCl bcc lattice with H^- atoms taking up the vertex positions of the underlying cube-like cages. The body-centered positions are occupied by a 1:1 mix of Mg^{2+} cations and H_2 molecules with slightly elongated bonds, as highlighted by the red and blue polyhedra in Fig. 4(a). The size mismatch between the two results in the hydrides forming different sized cages around them. The same $Cmcm$-MgH_4 structure was discovered in evolutionary runs carried out at 100 and 200 GPa, and phonon calculations at 100 GPa showed it was dynamically stable.

Interestingly, the lowest enthalpy $I4/mmm$-symmetry CaH_4 structure found using the particle-swarm optimization technique[56] in a recent study[20] can be described the same way as $Cmcm$-MgH_4. The difference between the two is the manner in which the cations and the H_2 molecules are distributed: in CaH_4 they are dispersed homogeneously, but in MgH_4, they are arranged into interwoven zigzag chains. Additionally, the hydride cages are more distorted in the MgH_4 structure with the smallest face which surrounds an Mg^{2+} being the one which links one magnesium cation to another. Actually, the structure can also be viewed as sheets of MgH_2 with H_2 molecules trapped in the larger gaps between the sheets, one such sheet is shown at the right of Fig. 4(a).

Within PBE, the total density of states of $Cmcm$-MgH_4 at 100 GPa is quite small; in fact it is lower than that of the $I4/mmm$ analog. The former is 42 meV/atom more stable than the latter at this pressure, but the volume of $I4/mmm$-MgH_4 is 0.04 $Å^3$ per atom smaller than that of $Cmcm$-MgH_4. The formation of the zigzag-like chains illustrated in Fig. 4(a) must therefore have a substantial impact on the electronic contribution to the enthalpy.

As the pressure increases from 100 to 300 GPa, the shortest distance between the metal cations decreases from 2.56 to 2.32 Å, and the Mg $2p$ core bands broaden from 0.19 to 0.58 eV due to core overlap. The shortest Mg–H^- distance decreases from 1.74 to 1.55 Å, as does the Mg-H_2 separation (1.92/1.68 Å). The molecular H_2 bonds lengthen somewhat from 0.78 Å to 0.79 Å. This is slightly longer than
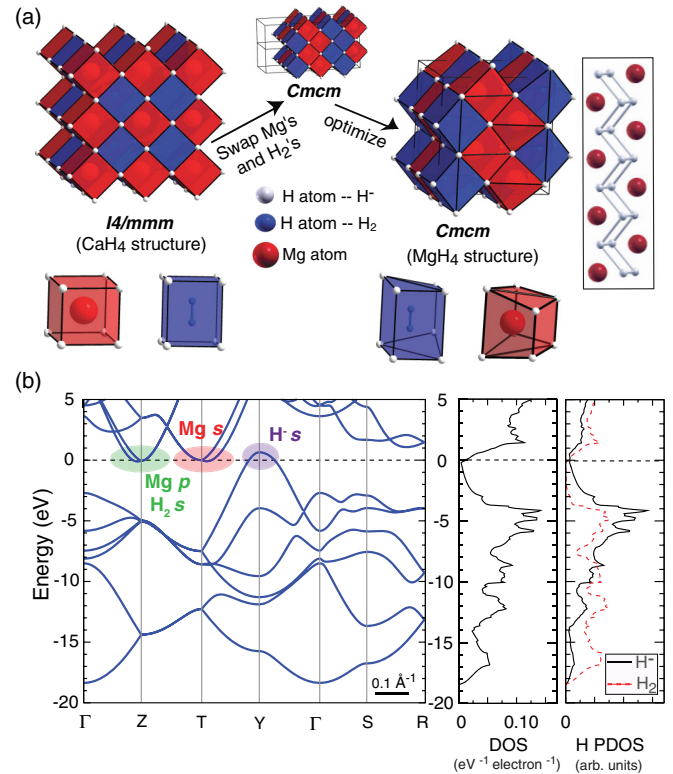

FIG. 4. (Color online) (a) A schematic illustration of the structural similarity between $Cmcm$-MgH_4 (right) and the $I4/mmm$-symmetry CaH_4 structure from Ref. 20 (left). The hydride cages around Mg^{2+}/Ca^{2+} and the H_2 molecules are colored red and blue, respectively.[57] (b) The PBE electronic band structure of MgH_4 at 100 GPa. The character of the bands which cross the Fermi level is highlighted. Also shown on the right are the total electronic and hydrogen site-projected densities of states (DOS).

the intramolecular distance in pure compressed H_2 at these pressures, 0.73 and 0.75 Å, respectively.

Since MgH_4 contains H^- units, it becomes metallic as a result of pressure induced band broadening and eventual overlap, like LiH_2 and NaH_9. Metallization occurs within PBE already by 20 GPa, even though $Cmcm$-MgH_4 is not stable with respect to decomposition into H_2 and MgH_2 at this pressure. A band displaying H^-s character rises above E_F at the Y point, whereas bands exhibiting predominantly Mg sp and a little bit of H_2 σ^* character fall below it at the Z and T points [see Fig. 4(b)]. Calculations using the HSE06 functional increase the metallization pressure to $\sim$150 GPa.

D. MgH_{12} and MgH_{16}: the $H_2^{\delta-}$ belt

The absence of H^- anions in the other structures lying on the convex hull at 200 GPa, MgH_{12} and MgH_{16}, has important consequences for their electronic structure. The hydrogenic sublattices of these phases are composed solely of $H_2^{\delta-}$ molecules with slightly stretched bonds, just like the CaH_{12} structure predicted in a previous study.[20] The presence of hydridic hydrogens in systems with a small mole fraction of hydrogen, and their absence in phases with a high hydrogen content was rationalized by Wang and co-workers by considering the formal number of "effectively added electrons"
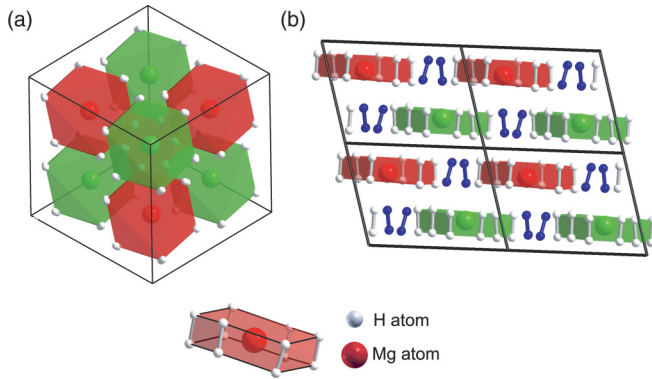
FIG. 5. (Color online) (a) A $2 \times 2 \times 2$ supercell of $R3$–MgH_{12} where the polyhedral units are highlighted to emphasize the $ABCABC...$ close-packed arrangement. The MgH_{12} building blocks are colored such that the red polyhedra all lie in the same plane. (b) A supercell of P-1-MgH_{16}. The MgH_{12} building blocks are colored to emphasize the similarity to the structure in (a). The blocks colored red or green lie in the same plane, and the hydrogens colored in blue do not belong to an MgH_{12} building block.[57]

FIG. 6. (Color online) The PBE valence densities of states of (a) MgH_{12} and (b) MgH_{16}. Note that the Fermi level lies just below (directly after) a sharp peak in the DOS in MgH_{12} at 140 GPa (MgH_{16} at 130 GPa).

(EAE), which are donated from the alkaline earth metal valence bands into the H_2 σ^* bands[20] for various CaH_n stoichiometries. If the EAE is small, the dihydrogen bond simply stretches as a result of the population of H_2 σ^*, and hydridic hydrogens are not formed. If the EAE is large enough, the molecule dissociates into two H^- units.

The most stable MgH_{12} structure found in our evolutionary searches had $R3$ symmetry and was shown to be dynamically stable at 140 GPa. The hexagonal building block for this phase consists of an Mg^{2+} cation surrounded by six $H_2^{-1/3}$ molecules, as illustrated in Fig. 5(a). The dihydrogen molecules in these hexagons appear to arrange in a "belt" around the metal cation in a side-on fashion. The hexagons are tiled in parallel sheets forming an $ABCABC...$ close-packed structure. This description is, however, somewhat misleading as the distance between Mg^{2+} and a hydrogen atom within the MgH_{12} building block is comparable to the shortest distance between the metal ion and a hydrogen atom in a different building block. For example, the intra and interbuilding block Mg-H measurements are 1.76 and 1.81 Å, respectively, at 140 GPa. The dihydrogen bonds in MgH_{12} are substantially elongated to 0.82 and 0.81 Å at 140 and 300 GPa, when compared with the typical bond lengths of pure H_2 at these pressures (0.74/0.75 Å). A gas phase geometry optimization on a $H_2^{-1/3}$ molecule at 1 atm showed that the bond stretched from 0.75 to 0.79 Å. So the expansion of the H–H bond observed in MgH_{12} is consistent with the partial filling of the H_2 σ^* bands.

The lowest enthalpy MgH_{16} configuration we found, which exhibited P-1 symmetry and was dynamically stable at 130 GPa, could be thought of as being made up of similar MgH_{12} units with excess $H_2^{\delta-}$ molecules stuffed between the hexagons, as illustrated in Fig. 5(b). These "interstitial" dihydrogens lie on top of the Mg^{2+} cations in the MgH_{12} building blocks. The intramolecular distance in $H_2^{-1/4}$ at 1 atm was calculated as being 0.78 Å, whereas the bond lengths of the dihydrogens in MgH_{16} range from 0.76 to 0.85 Å at 130 GPa, with the interstitial hydrogen molecules being shorter
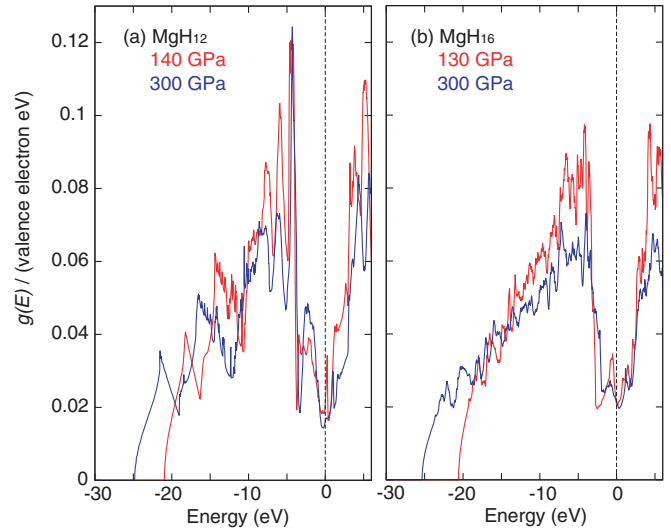
(0.76–0.78 Å) than those in the belt (0.79–0.85 Å). The unequal bond lengths in the $H_2^{\delta-}$ units may be a result of different charge states, or be due to their local bonding environments, or both.[58] As the pressure increases, the intramolecular H-H bond lengths decrease, with the interstitial and belt hydrogens measuring 0.74–0.76 Å and 0.78–0.84 Å, respectively, at 300 GPa.

Since MgH_{12} and MgH_{16} are metallic as a result of the partial filling of the H_2 σ^* bands like LiH_6, they have a high density of states at E_F, see Fig. 6. Both phases remain good metals upon compression up to at least 300 GPa, and the Mg $2p$ bands broaden only slightly to $\sim$0.15–0.2 eV at 300 GPa as a result of core overlap. A comparison of the DOS of MgH_{12} at 140 GPa calculated with PBE and the HSE06 screened hybrid functional showed that latter valence DOS was slightly broader (as expected for metallic systems),[59,60] and the core Mg $2p$ bands shifted to lower energies. However, the $g(E_F)$ computed with the two functionals was essentially the same (see the SI). This is in line with our previous results, which showed that $g(E_F)$ is relatively insensitive to the choice of the functional in sodium polyhydrides that did not contain hydridic hydrogens.[14] The nearly free-electron-like valence bands of MgH_{12} and MgH_{16} exhibit primarily H s character, with a little bit of Mg sp spanning throughout. Nonetheless, the computed DOS of these structures match quite well with a hypothetical system where the metal cations have been removed, the $(H_{12})^{2-}$ and $(H_{16})^{2-}$ lattices, suggestive of almost full ionization of the Mg valence $3s$ electrons into the H_2 σ^* bands.

E. The MgH_{12} building blocks

A number of MH_{12} clusters, where M is a transition metal atom, have been predicted as being stable in the gas phase by quantum chemical calculations.[61] Moreover, $WH_4(H_2)_4$, which contains four hydridic hydrogens and four dihydrogens bonded to the metal center in a side-on fashion, has been made in a neon matrix.[62] Unsurprisingly, molecular
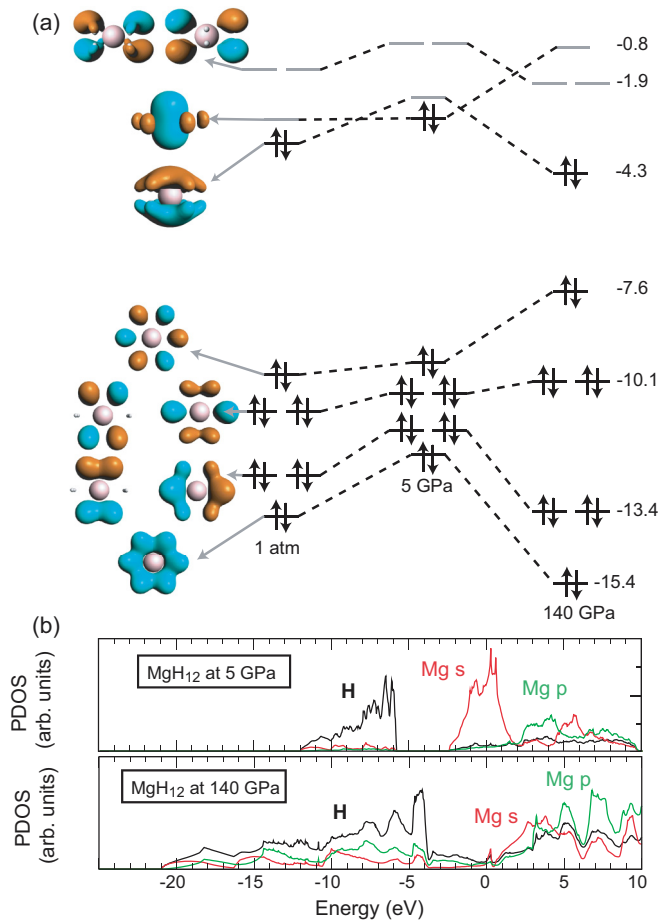
FIG. 7. (Color online) (a) Calculated molecular orbital level diagram of an MgH_{12} cluster when optimized in the gas phase at 1 atm (left) and in the geometry which it adopts in the $R3$-MgH_{12} solid at 5 GPa (center) and 140 GPa (right). The energies of the MOs at 140 GPa are given to the right in electron volts. (b) Calculated site-projected densities of states of $R3$-MgH_{12} at 5 and 140 GPa.

calculations on both the optimized MgH_{12} building blocks as well as $(MgH_{12})^{2+}$ with D_{6h} symmetry revealed numerous imaginary frequencies, so these clusters will not be stable at 1 atm. Nonetheless, it is instructive to compare the electronic structure of the MgH_{12} building block with the DOS computed for $R3$-MgH_{12} at various pressures.

Whereas in an optimized MgH_{12} cluster the Mg-H and intramolecular H-H distances were calculated as being 2.20 and 0.79 Å, these values measure 2.34–2.58/1.76–1.78, and 0.79/0.82 Å in $R3$-MgH_{12} at 5/140 GPa. So the gas phase cluster is actually a little bit more "compressed" than the building block within the solid at 5 GPa. The energy level diagrams and canonical molecular orbitals (MOs) of these clusters are illustrated in Fig. 7(a). The six MOs lowest in energy resemble the canonical MOs of benzene, except that they do not contain a node which bisects the dihydrogen molecules. A large gap is found between the highest occupied molecular orbital (HOMO) and HOMO-1 of the optimized cluster, but a small gap separates the HOMO and lowest unoccupied molecular orbital (LUMO). The HOMO-HOMO-1 gap decreases as the cluster is compressed, as do the

analogous sets of bands in the extended system, as illustrated in Fig. 7(b).

The frontier orbitals of the 1-atm cluster contain substantial character arising from H, and the HOMO also has an important contribution from the Mg $3p$ and the LUMO from the Mg $3s$ orbitals. Our fragment orbital analysis[63] shows that the LUMO + 1 contains primarily H character with less than 4% of Mg $3d$ states mixed in. In the "less-compressed," cluster extracted from the solid at 5 GPa, the frontier orbitals swap positions so that the HOMO displays Mg $3s$ and the LUMO Mg $3p$ character. This is in line with the projected densities of states, which illustrate that the predominant contribution around the Fermi level is due to Mg s at 5 GPa. At 140 GPa, the gap between the hydrogenic and the metallic bands between -6 to -3 eV closes in the solid, and the HOMO and HOMO-1 orbitals in the cluster come closer together in energy. Moreover, as a result of the pressure induced $s \rightarrow p$ transition in Mg, the states around the Fermi level contain about an equal amount of Mg s and p character. In the cluster, the energy ordering of the molecular orbitals also changes, so that the HOMO is more Mg p-like, and the LUMO displays primarily H s character. So the gas phase clusters are able to mimic some of the essential features of the projected DOS of the solid at different pressures.

F. Superconductivity in the polyhydrides

Our computations have estimated the T_c of the classic alkaline earth hydride, $P6_3/mmc$-MgH_2, as being $\sim$20 K at 180 GPa. We wondered what the T_c of the aforementioned hydrogen-rich phases would be in comparison, and if T_c would be influenced by the hydrogenic sublattice of the polyhydride. Computations have been carried out on $Cmcm$-MgH_4 and $R3$-MgH_{12} at 100 and 140 GPa, respectively, since these are pressures slightly larger than when ΔH_F was computed as becoming negative, and since both systems were found to be metallic within PBE at these pressures.

Within PBE the density of states at the Fermi level of $Cmcm$-MgH_4 at 100 GPa is comparable to the one calculated for ζ-MgH_2 at 180 GPa. The total EPC parameter is nearly 28% larger, however. In both phases, the low-frequency modes that are mostly due to the vibrations of the Mg atoms contribute $\sim$0.2 to the total λ; compare Figs. 8 and 2. The main reason why the overall EPC parameter is larger for the polyhydride than the classic hydride is a result of the total coupling provided by the modes between $\sim$500–2500 cm^{-1}, which are primarily due to the motions of the hydrogen atoms. Whereas the classic hydride contains only hydridic hydrogens, there is an equal number of H_2 and H$^-$ hydrogens in MgH_4. The H_2 vibron, located around 3500 cm^{-1} contributes only 1.5% to the total coupling strength in the polyhydride. This is not surprising, since the bands crossing the Fermi level displayed only a small amount of H_2 s character. Despite the higher λ that MgH_4 has as compared to MgH_2, the prefactor in the modified McMillan equation, ω_{ln}, is calculated as being 15% smaller so the total T_c of MgH_4 is estimated as being $\sim$14 K higher than that of the classic alkaline earth hydride.

Despite the increased hydrogen content and higher density of states at the Fermi level, the total EPC parameter of $R3$-MgH_{12} at 140 GPa is almost the same as of $Cmcm$–MgH_4
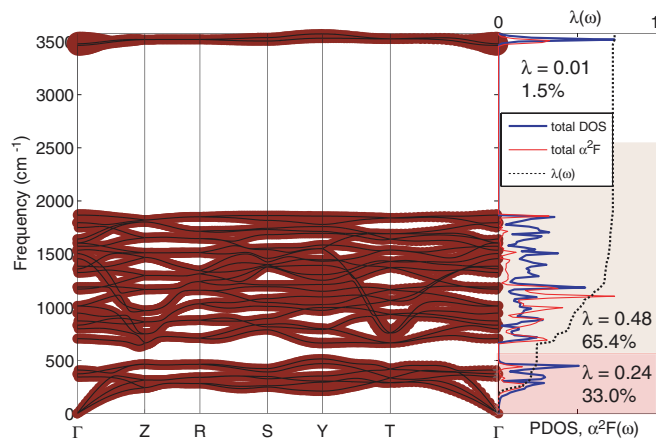
FIG. 8. (Color online) Phonon band structure, phonon density of states and the Eliashberg spectral function, $\alpha^2F(\omega)$, of MgH$_4$ at 100 GPa. Circles indicate the phonon linewidth with a radius proportional to the strength. At this pressure, $\lambda = 0.74$, $\omega_{ln} = 941$ K, and $T_c = 29$–37 K assuming $\mu^* = 0.13$–0.1.

at 100 GPa. However, a comparison of the $\lambda(\omega)$ in Fig. 8 and Fig. 9 shows that the relative contributions to the overall λ are quite different in the two polyhydrides. MgH$_{12}$ does not contain any hydridic hydrogens, and is metallic because of the partial filling of the H$_2$ σ^* bands. In contrast to what was found for MgH$_4$, the H$_2$ vibron contributes about 11.1% to the total λ. This corresponds quite well to the 11.3% calculated for a compressed KH$_6$ phase[19] whose hydrogenic sublattice only contained H$_2^{\delta-}$ motifs. The EPC associated with the low-frequency modes below 400 cm^{-1}, which are dominated by the motions of the heavier metal atoms, is about a third of the amount calculated for the phases containing H$^-$ units. The main contribution to λ, 79%, arises from the intermediate frequency regime, which is primarily due to the H$_2$ motions. The reason why the T_c of MgH$_{12}$ is estimated as being ~20 K higher than that of MgH$_4$ is due to the larger ω_{ln}.
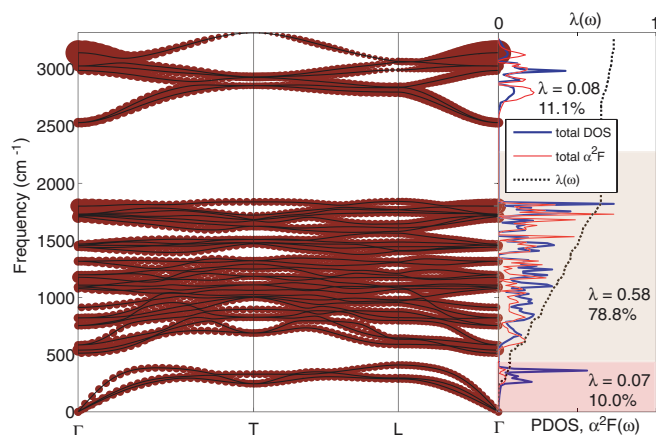

FIG. 9. (Color online) Phonon band structure, phonon density of states, and the Eliashberg spectral function, $\alpha^2F(\omega)$, of MgH$_{12}$ at 140 GPa. Circles indicate the phonon linewidth with a radius proportional to the strength. At this pressure, $\lambda = 0.73$, $\omega_{ln} = 1554$ K, and $T_c = 47$–60 K assuming $\mu^* = 0.13$–0.1.

Unfortunately, the computational expense precluded us from calculating the EPC parameter of compressed $P - 1$-MgH$_{16}$, or from exploring the pressure dependence of T_c.

The values we calculate for the total EPC parameter and the T_c of the magnesium polyhydrides falls within the range of 0.5–1.6 and 10–139 K, respectively, computed for a number of hydrogen-rich systems.[20] We show that comparable λ values may be obtained for polyhydrides with very different hydrogenic sublattices, but their ω_{ln} and therefore T_c may differ. The magnesium polyhydrides are predicted to have a larger T_c than MgH$_2$ under pressure, and phases with a larger mole percent ratio will likely have a higher T_c.

IV. CONCLUSIONS

Evolutionary structure searches coupled with density functional theory calculations are used to predict the most stable structures and stoichiometries of the magnesium polyhydrides, MgH$_n$ with $n \geqslant 2$, under pressure. The thermodynamically stable structures found in this study have a hydrogenic sublattice containing H$^-$ anions and H$_2$ units (MgH$_4$), or H$_2$ molecules, which are less strongly bonded than those found in pure molecular hydrogen at 1 atm (MgH$_{12}$ and MgH$_{16}$).

Metallization in $P6_3/mmc$-MgH$_2$ occurs as a result of an H$^-$ s band rising above, and a Mg sp band falling below the Fermi level. T_c is estimated as being between 16–23 K at 180 GPa, with a sizable contribution to the total electron phonon coupling parameter arising from vibrations related to both the hydrogen and magnesium atoms.

MgH$_4$, which starts to become thermodynamically stable with respect to decomposition into MgH$_2$ and H$_2$ near 100 GPa is found to contain one H$_2$ molecule and two hydridic hydrogens per Mg^{2+} cation. Metallization occurs as a result of pressure-induced band gap closure, but the density of states at the Fermi level is quite low. Around 120 GPa other stoichiometries, whose hydrogenic sublattices contain only H$_2^{\delta-}$ molecules with slightly stretched bonds, emerge as being thermodynamically stable. MgH$_{12}$ and MgH$_{16}$ are metallic in part as a result of the partial filling of the H$_2$ σ^* bands and have a high density of states at the Fermi level. Their electronic structure at various pressures can be traced back to the molecular orbital diagram of their building block, the MgH$_{12}$ cluster. Despite the very different hydrogenic sublattices, both MgH$_4$ and MgH$_{12}$ are found to have similar electron phonon coupling parameters. The main reason why the T_c of MgH$_{12}$ at 140 GPa is calculated as being larger than that of MgH$_4$ at 100 GPa, 47–60 K versus 29–37 K assuming typical values of μ^*, is because of the larger average logarithmic frequency computed for MgH$_{12}$.

*ezurek@buffalo.edu

[1] E. Wigner and H. B. Huntington, J. Chem. Phys. **3**, 764 (1935).

[2] C. J. Pickard and R. J. Needs, Nat. Phys. **3**, 473 (2007).

[3] H. Liu, H. Wang, and Y. Ma, J. Phys. Chem. C **116**, 9221 (2012).

[4] J. M. McMahon and D. M. Ceperley, Phys. Rev. Lett. **106**, 165302 (2011).

[5] C. S. Zha, Z. Liu, and R. J. Hemley, Phys. Rev. Lett. **108**, 146402 (2012).

[6] R. T. Howie, C. L. Guillaume, T. Scheler, A. F. Goncharov, and E. Gregoryanz, Phys. Rev. Lett. **108**, 125501 (2012).

[7] M. I. Eremets and I. A. Troyan, Nat. Mater. **10**, 927 (2011).

[8] I. Amato, Nature (London) **486**, 174 (2012).

[9] H. Liu, L. Zhu, W. Cui, and Y. Ma, J. Chem. Phys. **137**, 074501 (2012).

[10] C. J. Pickard, M. Martinez-Canales, and R. J. Needs, Phys. Rev. B **85**, 214114 (2012).

[11] P. Cudazzo, G. Profeta, A. Sanna, A. Floris, A. Continenza, S. Massidda, and E. K. U. Gross, Phys. Rev. Lett. **100**, 257001 (2008).

[12] J. M. McMahon and D. M. Ceperley, Phys. Rev. B **84**, 144515 (2011).

[13] E. Zurek, R. Hoffmann, N. W. Ashcroft, A. R. Oganov, and A. O. Lyakhov, Proc. Natl. Acad. Sci. USA **106**, 17640 (2009).

[14] P. Baettig and E. Zurek, Phys. Rev. Lett. **106**, 237002 (2011).

[15] J. Hooper and E. Zurek, Chem. Eur. J. **18**, 5013 (2012).

[16] J. Hooper and E. Zurek, J. Phys. Chem. C **116**, 13322 (2012).

[17] A. Shamp, J. Hooper, and E. Zurek, Inorg. Chem. **51**, 9333 (2012).

[18] J. Hooper, B. Altintas, A. Shamp, and E. Zurek, J. Phys. Chem. C (2013), doi: 10.1021/jp311571n.

[19] D. Zhou, X. Jin, X. Meng, G. Bao, Y. Ma, B. Liu, and T. Cui, Phys. Rev. B **86**, 014118 (2012).

[20] H. Wang, J. S. Tse, K. Tanaka, T. Iitaka, and Y. Ma, Proc. Natl. Acad. Sci. USA **109**, 6463 (2012).

[21] D. C. Lonie and E. Zurek, Comput. Phys. Commun. **182**, 372 (2011).

[22] D. C. Lonie and E. Zurek, Comput. Phys. Commun. **183**, 690 (2012).

[23] Spglib, http://spglib.sourceforge.net/.

[24] G. Kresse and J. Hafner, Phys. Rev. B **47**, 558 (1993).

[25] J. P. Perdew, K. Burke, and M. Ernzerhof, Phys. Rev. Lett. **77**, 3865 (1996).

[26] P. E. Blöchl, Phys. Rev. B **50**, 17953 (1994).

[27] A. V. Krukau, O. A. Vydrov, A. F. Izmaylov, and G. E. Scuseria, J. Chem. Phys. **125**, 224106 (2006).

[28] H. Liu, W. Cui, and Y. Ma, J. Chem. Phys. **137**, 184502 (2012).

[29] A. M. Teweldeberhan, J. L. DuBois, and S. A. Bonev, Phys. Rev. B **86**, 064104 (2012).

[30] B. Boates and S. A. Bonev, Phys. Rev. B **83**, 174114 (2011).

[31] C. J. Pickard and R. J. Needs, Phys. Rev. Lett. **102**, 146401 (2009).

[32] Phonopy, http://phonopy.sourceforge.net/.

[33] P. Giannozzi, S. Baroni, N. Bonini, M. Calandra, R. Car, C. Cavazzoni, D. Ceresoli, G. L. Chiarotti, M. Cococcioni, I. Dabo *et al.*, J. Phys.: Condens. Matter **21**, 395502 (2009).

[34] J. P. Perdew and A. Zunger, Phys. Rev. B **23**, 5048 (1981).

[35] B. B. Karki, R. M. Wentzcovitch, S. de Gironcoli, and S. Baroni, Phys. Rev. B **62**, 14750 (2000).

[36] M. Methfessel and A. T. Paxton, Phys. Rev. B **40**, 3616 (1989).

[37] P. B. Allen and R. C. Dynes, Phys. Rev. B **12**, 905 (1975).

[38] Amsterdam Density Functional Program Package, http://www.scm.com/.

[39] See Supplemental Material at http://link.aps.org/supplemental/10.1103/PhysRevB.87.054107 for the convex hull plot, structural parameters, LMTO fat bands, select densities of states and the dependence of Tc on the Coulomb Pseudopotential.

[40] O. K. Andersen and O. Jepsen, Phys. Rev. Lett. **53**, 2571 (1984).

[41] P. Vajeeston, S. Sartori, P. Ravindran, K. D. Knudsen, B. Hauback, and H. Fjellvag, J. Phys. Chem. C **116**, 21139 (2012).

[42] P. Vajeeston, P. Ravindran, M. Fichtner, and H. Fjellvag, J. Phys. Chem. C **116**, 18965 (2012).

[43] J. M. Reich, L. L. Wang, and D. D. Johnson, J. Phys. Chem. C **116**, 20315 (2012).

[44] E. N. Koukaras, A. D. Zdetsis, and M. M. Sigalas, J. Am. Chem. Soc. **134**, 15914 (2012).

[45] A. C. Buckley, D. J. Carter, D. A. Sheppard, and C. E. Buckley, J. Phys. Chem. C **116**, 17985 (2012).

[46] P. Vajeeston, P. Ravindran, B. C. Hauback, H. Fjellvag, A. Kjekshus, S. Furuseth, and M. Hanfland, Phys. Rev. B **73**, 224102 (2006).

[47] P. Vajeeston, P. Ravindran, A. Kjekshus, and H. Fjellvag, Phys. Rev. Lett. **89**, 175506 (2002).

[48] J. S. Tse, Z. Song, Y. Yao, J. S. Smith, S. Desgrenniers, and D. D. Klug, Solid State Commun. **149**, 1944 (2009).

[49] C. Chen, F. Tian, L. Wang, D. Duan, T. Cui, B. Liu, and G. Zou, J. Phys.: Condens. Matter **22**, 225401 (2010).

[50] J. S. Tse, D. D. Klug, S. Desgreniers, J. S. Smith, R. Flacau, Z. Liu, J. Hu, N. Chen, and D. T. Jiang, Phys. Rev. B **75**, 134108 (2007).

[51] J. S. Smith, S. Desgrenniers, D. D. Klug, and J. S. Tse, Solid State Commun. **149**, 830 (2009).

[52] C. Zhang, X. J. Chen, R. Q. Zhang, and H. Q. Lin, J. Phys. Chem. C **114**, 14614 (2010).

[53] J. Nagamatsu, N. Nakagawa, T. Muranaka, Y. Zenitani, and J. Akimitsu, Nature (London) **410**, 63 (2001).

[54] H. J. Choi, D. Roundy, H. Sun, M. L. Cohen, and S. G. Louie, Nature (London) **418**, 758 (2002).

[55] J. Hooper, P. Baettig, and E. Zurek, J. Appl. Phys. **111**, 112611 (2012).

[56] Y. Wang, J. Lv, L. Zhu, and Y. Ma, Phys. Rev. B **82**, 094116 (2010).

[57] Pictures created using ENDEAVOUR 1.7, Crystal Impact, Bonn, Germany (2012); http://www.crystalimpact.com/endeavour [www.crystalimpact.com], E-mail: info@crystalimpact.com.

[58] V. Labet, R. Hoffmann, and N. W. Ashcroft, J. Chem. Phys. **136**, 074502 (2012).

[59] A. Biller, I. Tamblyn, J. B. Neaton, and L. Kronik, J. Chem. Phys. **135**, 164706 (2011).

[60] J. Paier, M. Marsman, K. Hummer, G. Kresse, I. C. Gerber, and J. G. Angyan, J. Chem. Phys. **124**, 154709 (2006).

[61] L. Gagliardi and P. Pyykkö, J. Am. Chem. Soc. **126**, 15014 (2004).

[62] X. Wang, L. Andrews, I. Infante, and L. Gagliardi, J. Am. Chem. Soc. **130**, 1972 (2008).

[63] G. te Velde, F. M. Bickelhaupt, E. J. Baerends, C. Fonseca Guerra, S. J. A. van Gisbergen, J. G. Snijders, and T. Ziegler, J. Comput. Chem. **22**, 931 (2001).